MoO₃ Nanostructured Electrodes Prepared via Hydrothermal Process for Lithium Ion Batteries

Biao Han, Kyung-Hoon Lee, Young-Woo Lee, Si-Jin Kim, Han-Chul Park, Bo-Mi Hwang,
Da-Hee Kwak, and Kyung-Won Park[*]

Department of Chemical Engineering, Soongsil University, Seoul 156-743, Republic of Korea.
[*]E-mail: kwpark@ssu.ac.kr

We demonstrated the use of MoO₃ nanostructure electrodes for lithium ion batteries, synthesized by the hydrothermal process with different concentrations of nitric acid. As the concentration of nitric acid increased, the electrodes showed phase transition from the metastable hexagonal MoO₃ (h-MoO₃) to the stable orthorhombic MoO₃ (α-MoO₃). The electrodes prepared in 0.1 and 1 M HNO₃ exhibited rod-shaped h-MoO₃ structures. However, the electrode prepared in 4 M HNO₃ exhibited a mixed configuration of rod-shaped h-MoO₃ and belt-type α-MoO₃ structure. Finally, the electrode prepared in 5 M HNO₃ displayed a complete transition to the belt-type α-MoO₃ structure. The single-crystalline nature of α-MoO₃ nanobelts prepared in 5.0 M HNO₃ was clearly observed by field-emission transmission electron microscopy, demonstrating that the MoO₃ nanobelts were also grown along the [001] direction. The single-crystalline α-MoO₃ nanobelts showed improved charge capacity and high rate performance due to their relatively large specific surface area, low transport resistance, and the high lithium ion diffusion coefficient of the nanostructure electrode.

1. INTRODUCTION

In rechargeable Li-ion batteries (LIBs), the active electrodes store and release electrochemical energy by the insertion and extraction of Li-ions and electrons in host structures.[1-5] Due to small particle size and high surface area, the use of nanomaterials could improve the electrochemical properties of LIBs compared to their bulky counterparts by introducing new active reactions, decreasing the path length for Li-ion and electron transport, and increasing the interfacial contact area.[6] Specifically, transition metal oxides as an active material have been extensively studied for LIBs because of their high capacity, cyclability, and low cost. [7-9]

Among them, molybdenum trioxide (MoO_3) has gained attention as a promising candidate for LIB with high energy density due to its unique layered orthorhombic crystal structure.[10] One polytypic phase for MoO_3 is a thermodynamically stable orthorhombic MoO_3 (α-MoO_3) phase, while it also has a metastable monoclinic MoO_3 (β-MoO_3) and hexagonal MoO_3 (h-MoO_3) phases.[11,12] The α-MoO_3 phase exhibits an anisotropic structure with layers parallel to the (010) crystal plane, which consist of two sublayers, and each sublayer is formed by corner-sharing octahedrons along the [001] and [100] directions. The two sublayers share the edges of the octahedron along the [001] direction to form a layer. Recently, a number of processes have been developed to synthesize well-controlled MoO_3 nanocrystals.[13,14]

In the case of one-dimensional (1-D) nanostructures, the synthesis of 1-D nanostructured electrode materials has attracted intensive attention to increase the performance of LIBs.[15-17] The energy density, cycling life, and safety of rechargeable LIBs have been dramatically influenced by the particle size, structural modification, and morphology of the active materials in the electrode.[3] For example, $LiCoO_2$ fibers and tubes showed a high initial discharge capacity with improved behavior of Li+ ions.[18,19] Nanostructured V_2O_5 electrodes exhibited larger surface area and shorter diffusion paths for Li^+ intercalation than the conventional electrode.[20] Previously, MoO_3 nanostructures with various morphologies were also prepared. Li and co-workers prepared MoO_3 nanobelts and nanotubes by infrared irradiation heating of a Mo foil.[21] Li et al. synthesized single-crystal MoO_3 nanobelts through a solution approach.[22] Lou et al. synthesized MoO_3 nanorods and complex MoO_3 nanostructures via a hydrothermal method, combined with the manipulation of crystal growth directions.[23] Although MoO_3 has been prepared in various morphologies, few attempts have been made to investigate the electrochemical lithium behaviour of the unique MoO_3 micro- or nanostructures.[24-28]

Herein, we synthesized MoO_3 electrodes for LIBs via a hydrothermal process, without the use of any surfactant or template, as a function of the concentration of nitric acid. The structural characterization of the MoO_3 electrodes was carried out using scanning electron microscopy (SEM), transmission electron microscopy (TEM), fast Fourier transform (FFT), and X-ray diffraction (XRD) analysis. To characterize the surface area of the electrodes, the Brunauer-Emmett-Teller (BET) curve was obtained using nitrogen sorption measurement. Charge-discharge and high rate curves of the electrodes were measured using lithium coin cells to evaluate the performance of the electrodes in LIBs.

2. EXPERIMENTAL

To construct molybdenum oxide nanostructure electrodes, ammonum molybdate tetrahydrate ((NH_4)$6Mo_7O_{24}$·$4H_2O$, Aldrich, 99.99 %) was dissolved with differenct concentrations (0.1-5 M) of HNO_3 (Nitric acid, Samchun chemical, 60%) under constant stirring at 25 ^{o}C for 1 h, then kept at 160 ^{o}C for 3 h in an autoclave. After the hydrothermal process, the resulting precipitate was cooled to room temperature, washed several times with ethanol and distilled water, and filtered. The MoO_3 nanostructure electrodes were dried in 50 ^{o}C oven.

The as-prepared samples were characterized by field-emission TEM using a Tecnai G2 F30 system operating at 300 kV. The TEM samples were prepared by placing a drop of the suspension in ethanol on a carbon-coated copper grid. SEM images were obtained on a JEOL JSM-6360A microscope operated at 20 kV. Structural analysis of the samples was carried out by XRD using a Bruker AXS D2 Phaser X-Ray Diffractometer with a Cu K_{α} ($\lambda = 0.15418$ nm) and a Ni filter. Nitrogen adsorption and desorption isotherms were measured at 77 K using a Micromeritics ASAP 2020. Before the adsorption measurements, all samples were outgassed at 473 K for 360 min in the port of the adsorption analyzer. The starting relative pressure was 0.995 P/P_o, and the ending relative pressure was 0.01 P/P_o.

The final electrodes were prepared by mixing 70 wt% MoO_3 as an active material, 20 wt% acetylene black as the conducting agent, and 10 wt% polyvinylidene fluoride (PVDF) as the binder. To obtain the slurry, several drops of N-methylpymolidinone were added to the mixture of MoO_3 powder with acetylene black and PVDF. The mixed slurries were cast onto a Cu foil as a current collector and dried in air at 100 ^{o}C for 12 h. The resulting electrodes (an area of 1.32 cm^2) were dried in 70 ^{o}C vacuum oven. The electrodes were then evaluated with respect to a lithium foil (FMC Corporation) as a counter electrode. Coin cells were assembled inside an Ar-filled glove box (< 5 ppm, H_2O and O_2). The positive and negative electrodes of the cells were separated by a porous polypropylene membrane (Wellcos) and an electrolyte solution consisting of 1.1 M $LiPF_6$ in ethylene carbonate: diethylcarbonate (1:1) solvent mixture (Techono Semichem).

The electrochemical properties of the assembled cells were recorded by obtaining the charge-discharge curves in a voltage range between 3.3 and 1.5 V. For charge-discharge tests, the coin cells were galvanostatically cycled between 3.3 and 1.5 V for 100 cycles at a current rate of 1 C. The charge-discharge measurements were also carried out at different current rates, from 0.5 to 5 C, in order to evaluate the C-rate performance. For electrochemical impedance spectroscopic measurements, a 5-mV excitation potential was applied to the cells, while the frequency ranged from 100 kHz to 10 mHz. All electrochemical measurements were carried out at 25 ^{o}C.

3. RESULTS AND DISCUSSION

Fig. 1 shows XRD patterns of the MoO_3 electrodes synthesized, as a function of HNO_3 concentration. The diffraction patterns of the electrodes prepared in 0.1 and 1 M HNO_3 (MoO_3-0.1M and MoO_3-1M) were those of hexagonal h-MoO_3 (Fig. 1(a) and (b)). The electrode prepared in 4 M HNO_3 (MoO_3-4M) exhibited a mixed phase of hexagonal h-MoO_3 and orthorhombic α-MoO_3 (Fig. 1(c)). On the other hand, the electrode prepared in 5 M HNO_3 (MoO_3-5M) displayed the pure orthorhombic α-MoO_3 phase. The unit cell parameters for MoO_3-5M were determined to be 3.96, 13.86, and 3.7 Å, which are identical to those of the bulk α-MoO_3 material (Fig. 1(d)). It is known that the h-MoO_3 phase is metastable, while the α-MoO_3 phase is thermodynamically stable. These results indicate that as the concentration of nitric acid in the hydrothermal process increased from 0.1 to 5 M, the electrodes exhibited a phase transition from the metastable h-MoO_3 to the stable α-MoO_3 crystalline structure. Fig. 2 shows SEM images of the MoO_3 electrodes prepared with different

concentrations of HNO_3. As can be seen in Fig. 2(a) and (b), MoO_3-0.1M and MoO_3-1M exhibited rod-shaped structures. However, MoO_3-4M exhibited a mixed configuration of rod-shaped and belt-type structure (Fig. 2(c)). Finally, MoO_3-5M displayed a complete belt-type structure (Fig. 2(d)). This shows that as the concentration of HNO_3 in the hydrothermal process increased, the electrodes exhibited a transition from the rod-type h-MoO_3 to the belt-type α-MoO_3.
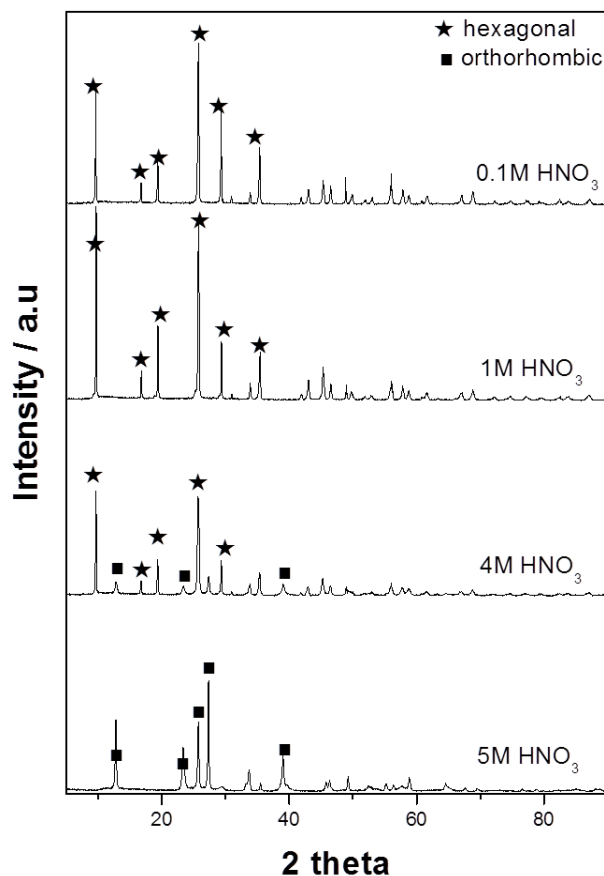

Figure 1. XRD patterns of MoO_3 electrodes prepared via hydrothermal process with different concentrations of HNO_3.

The length of the as-synthesized MoO_3-5M was calculated from Fig. 3 (a) and (b) to be ~5.7 μm. The belt widths varied in the range of a few hundred nm. A representative high-resolution TEM image and the corresponding FFT pattern of the MoO_3 nanobelt (Fig. 3(c)) confirmed the single-crystalline nature of the nanobelt, also demonstrating that the nanobelt growth occurred along the [001] direction. The BET curve was obtained to further characterize the surface are of MoO_3-5M, as shown in Fig. 3(d). The BET specific surface area of MoO_3-5M was ~16.7 m^2 g^{-1}. For comparison, commercial molybdenum trioxide (Comm-MoO_3, Sigma-Aldrich) powder of several μm in size, orthorhombic polycrystalline structure, and ~1.6 m^2 g^{-1} in BET surface area was also used (Fig. 4(a)-(d)).
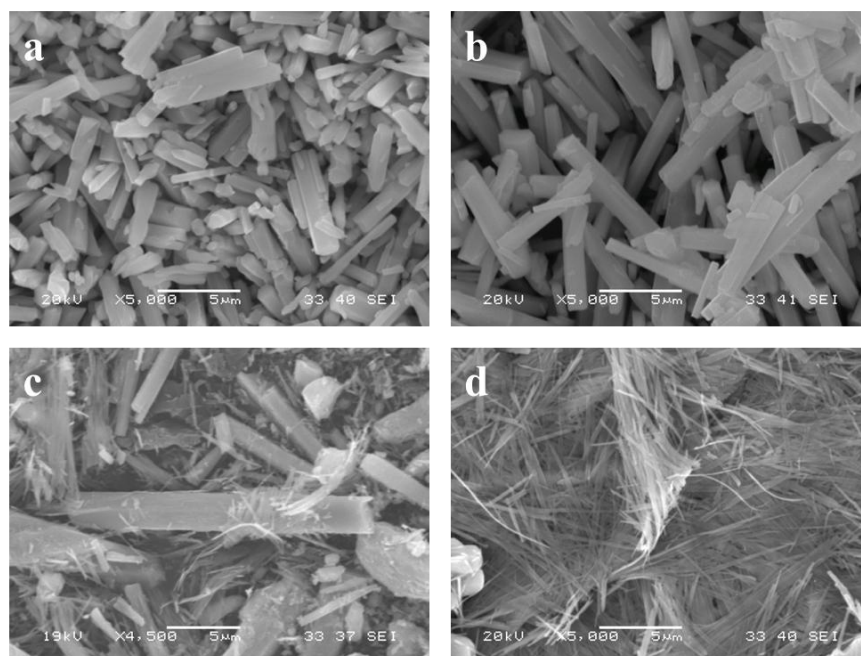
Figure 2. SEM images of MoO_3 electrodes prepared via hydrothermal process in (a) 0.1 M, (b) 1 M, (c) 4 M, and (d) 5 M HNO_3.
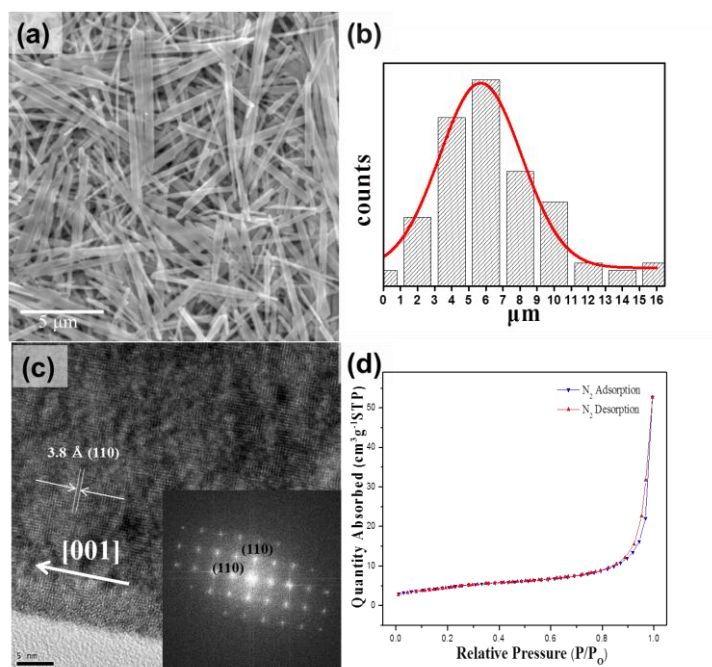

Figure 3. (a) SEM image (b) size distribution histogram, (c) HR-TEM image (The inset indicates the FFT pattern of the corresponding image.), and (d) N_2 gas sorption isotherm of MoO_3-5M.
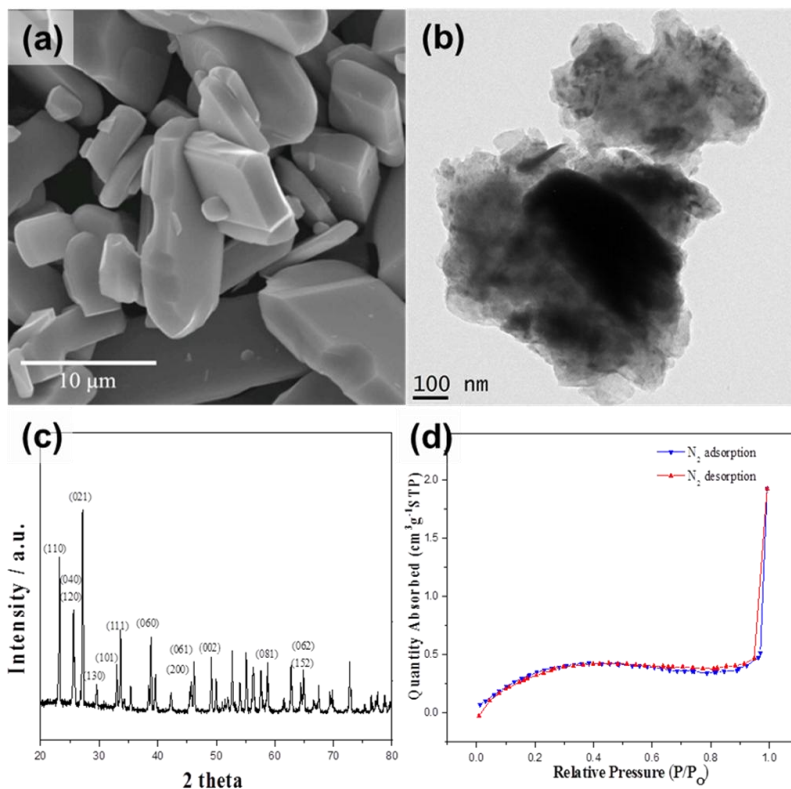
Figure 4. (a) SEM image, (b) TEM image, (c) XRD pattern, and (d) N_2 gas sorption isotherm of Comm-MoO_3.
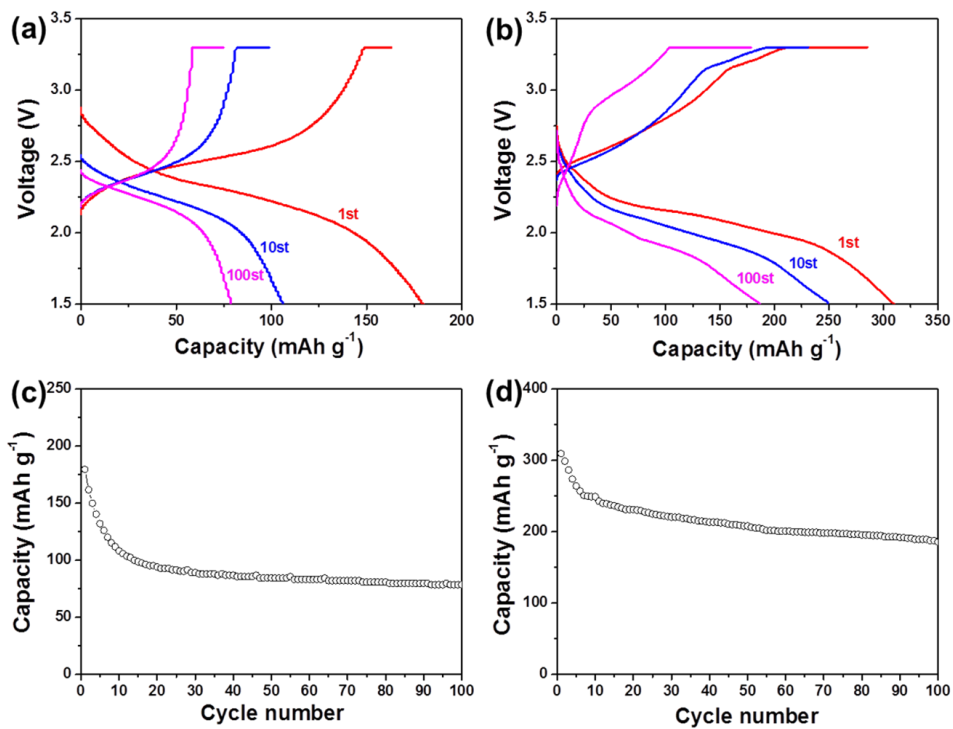

Figure 5. Charge-discharge curves and cycling performance of Comm-MoO_3 ((a),(c)) and MoO_3-5M ((b),(d)) for 100 cycles at 1 C.

The discharge-charge curves of MoO_3-5M and Comm-MoO_3 at a current density of 1 C are shown in Fig. 5(a) and (b). At the cycling rate of 1 C, the 1st discharge capacities of MoO_3-5M and Comm-MoO_3 were 309 and 179 mAh g^{-1}, respectively. The 10th discharge capacities of MoO_3-5M and Comm-MoO_3 were reduced to 249 and 108 mAh g^{-1}. At the 100th discharge, MoO_3-5M and Comm-MoO_3 had capacities of 186 and 78 mAh g^{-1}, respectively. The initial discharge capacity of MoO_3-5M was much larger than that of the previously reported MoO_3 electrodes.[6] As indicated in Fig. 5(c) and (d), MoO_3-5M exhibited much improvement in the performance up to 100 cycles with a reversible capacity of ~226 mAh g^{-1}, as compared to Comm-MoO_3 (~84 mAh g^{-1}). It is notable that the capacity of MoO_3-5M was larger at the 100th discharge than the initial value for Comm-MoO_3.

To investigate high rate performance of the electrodes, the discharge-charge curves were obtained for increasing current rates, from 0.5 to 5 C. As indicated in Fig. 6 (a) and (b), the respective specific discharge capacities of MoO_3-5M and Comm-MoO_3 were as follows: 276 and 141 mAh g^{-1} at 0.5 C; 222 and 93 mAh g^{-1} at 1 C; 158 and 72 mAh g^{-1} at 2 C; 90 and 53 mAh g^{-1} at 5 C. This demonstrated that MoO_3-5M displayed excellent high rate performance from 0.5 to 5 C. Furthermore, to investigate the high rate cycling performance of the electrodes, the discharge-charge rates were also increased stepwise from 0.5 to 5 C. As indicated in Fig. 6(c) and (d), even at current rates increased from 0.5 to 5 C, the MoO_3-5M displayed excellent high rate cycling properties. The remarkably large capacity of 251 mAh g^{-1} could be obtained when the current rate was returned to 0.5 C after 50 cycles at the different current rates.
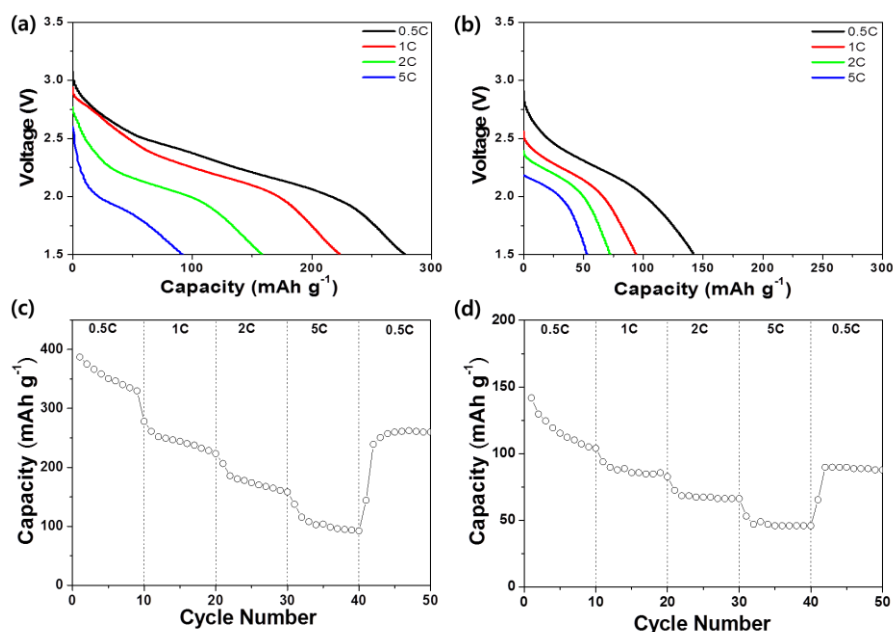

Figure 6. High rate performance of MoO_3-5M ((a),(c)) and Comm-MoO_3 ((b),(d)) with current rates varying from 0.5 C to 5 C.

Fig. 7(a) shows Nyquist plots of MoO_3-5M and Comm-MoO_3 between 100 kHz and 10 mHz. The value of the diameter of the semicircle on the Z_{real} axis is related to the charge transfer resistance

(R_{ct}). The values of R_{ct} of MoO$_3$-5M and Comm-MoO$_3$ were 82.0 and 133.9 Ω, respectively, demonstrating the much improved charge transport of MoO$_3$-5M. As indicated in Fig. 7(b), using the relationship between Z_{Re} and the square root of the frequency ($\omega^{-1/2}$) in the low frequency range (Eq. (1)), the Warburg impedance coefficients (σ_W) of MoO$_3$-5M and Comm-MoO$_3$ were calculated to be 3.86 and 4.15 Ω cm^2 s$^{-1/2}$, respectively.

$$Z_{Re} = R_e + R_{ct} + \sigma_W \, \omega^{-1/2} \qquad (1)$$
$$D = R^2T^2 \,/\, 2A^2n^4F^4C^2\sigma_W^2 \qquad (2)$$

From Eq. (2), the Li-ion diffusion coefficients of MoO$_3$-5M and Comm-MoO$_3$ were calculated to be 6.3×10^{-13} and 5.4×10^{-13} cm^2 s^{-1}, respectively, with MoO$_3$-5M exhibiting a faster Li-ion diffusion process. The improved lithium-ion intercalation properties of MoO$_3$-5M, such as high capacity and high rate performance, may be attributed to the relatively large specific surface area, low transport resistance, and high lithium ion diffusion coefficient of the 1-D nanostructure electrode.[29-31]
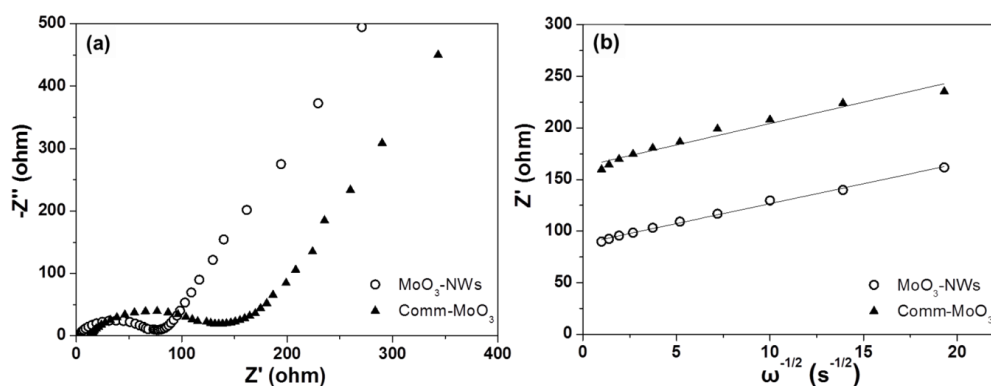

Figure 7. (a) Nyquist plots of MoO$_3$-5M and Comm-MoO$_3$ between 100 kHz and 10 mHz. (b) Relationship between Z_{Re} and $\omega^{-1/2}$ in the low frequency range.

4. CONCLUSIONS

We prepared MoO$_3$ nanostructure electrodes by means of the hydrothermal process, without the use of surfactant or template in different concentrations of HNO$_3$ solution. As the concentration of nitric acid increased, the electrodes exhibited a transition of the metastable h-MoO$_3$ rod-type structure to the stable orthorhombic α-MoO$_3$ belt structure. The as-prepared MoO$_3$ electrode prepared in 5 M HNO$_3$ exhibited a single-crystalline nanobelt grown along the [001] direction. The single-crystalline MoO$_3$ electrode displayed high charge capacity and excellent rate performance compared to Comm-MoO$_3$, facilitating lithium ion motion within due to low ionic transport resistance and high lithium ion diffusion coefficient in the nanostructure electrode.

References

1.   J.-M. Tarascon and M. Armand, *Nature,* 414 (2001) 359
2.   R. Mukherjee, R. Krishnan, T. -M. Lu and N. Koratkar, *Nano Energy,* 1 (2012) 518
3.   Q. Zhang, *Int. J. Electrochem. Sci.,* 8 (2013) 6457
4.   J. Li, J. Li, J. Luo, L. Wang and X. He, *Int. J. Electrochem. Sci.,* 6 (2011) 1550
5.   R. Ramachandran, V. Mani, S.-M. Chen, R. Saraswathi and B.-S. Lou, *Int. J. Electrochem. Sci.,* 8 (2013) 11680
6.   A. S. Aricò, P. Bruce, B. Scrosati, J. Tarascon and W. van Schalkwijk, *Nat. Mater.,* 4 (2005) 366
7.   G. Centi and S. Perathoner, *Eur. J. Inorg. Chem.,* 2009 (2009) 3851
8.   C. Liang, M. Gao, H. Pan, Y. Liu and M. Yan, *J. Alloys. Compd.,* 575 (2013) 246
9.   N. Nitta and G. Yushin, Part. Part. *Syst. Charact.,* 31 (2014) 317
10. S. -H. Lee, Y. -H Kim, R. Deshpande, P. A. Parilla, E. Whitney, D. T. Gillaspie, K. M. Jones, A. H. Mahan, S. Zhang and A. C. Dillon, *Adv. Mater.,* 20 (2008) 3627
11. J. W. Rabalais, R. J. Colton and A. M. Guzman, *Chem. Phys. Lett.,* 29 (1974) 131
12. L. Mai, B. Hu, W. Chen, Y. Qi, C. Lao, R. Yang, Y. Dai and Z. L. Wang, *Adv. Mater.,* 19 (2007) 3712
13. S. R. Dhage, M. S. Hassan and O. -B. Yang, *Mater. Chem. Phys.,* 114 (2009) 511
14. G. Li, L. Jiang, S. Pang, H. Peng and Z. Zhang, *J. Phys. Chem. B,* 110 (2006) 24472
15. J. Jiang, Y. Li, J. Liu and X. Huang, *Nanoscale,* 3 (2011) 45
16. K. Dewangan, N. N. Sinha, P. K. Sharma, A. C. Pandey, N. Munichandraiah and N. S. Gajbhiye, *CrystEngComm,* 13 (2011) 927
17. J. Ye, H. Zhang, R. Yang, X. Li and L. Qi, *Small,* 6 (2010) 296
18. Y. Gu, D. Chen and X. Jiao, *J. Phys. Chem. B,* 109 (2005) 17901
19. S. Amaresh, K. Karthikeyan, K. -J. Kim, J. -Y. An, S. -J. Cho, K. -Y. Chung, B. -W. Cho, K.-W. Nam and Y. -S. Lee, *J. Nanosci. Nanotechnol.,* 14 (2014) 7545
20. K. Lee, Y. Wang and G. Cao, *J. Phys. Chem. B,* 109 (2005) 16700
21. Y. B. Li, Y. Bando, D. Golberg and K. Kurashima, *Appl. Phys. Lett.,* 81 (2002) 5048
22. X. -L. Li, J. -F. Liu and Y. -D. Li, *Appl. Phys. Lett.,* 81 (2002) 4832
23. X. W. Lou and H. C. Zeng, *Chem. Mater.,* 14 (2002) 4781
24. C. Feng, H. Gao, C. Zhang, Z. Guo and H. Liu, *Electrochim. Acta,* 93 (2013) 101
25. Q. Xia, H. Zhao, Z. Du, J. Wang, T. Zhang, J. Wang and P. Lv, *J. Power Sources,* 226 (2013) 107
26. C. L. Liu , Y. Wang, C. Zhang, X. –S. Li and W. –S. Dong, *Mater. Chem. Phys.,* 143 (2014) 1111
27. R. Nadimicherla, Y. Liu, K. Chen and W. Chen, *Solid State Sci.,* 34 (2014) 43
28. A. Chithambararaj, N. Rameshbabu and A. C. Bose, Sci. *Adv. Mater.,* 6 (2014) 1302
29. L. Noerochim, J. –Z. Wang, D. Wexler, Z. Chao and H. –K. Liu, *J. Power Sources*, 228 (2013) 198
30. J. Zhou, H. Song, B. Fu, B. Wu and X. Chen, *J. Mater. Chem.,* 20 (2010) 2794
31. B. -M. Hwang, S. -J. Kim, Y. -W. Lee, B. Han, S. -B. Kim, W. -S. Kim and K. -W. Park, *Int. J. Electrochem. Sci.,* 8 (2013) 9449